Use of laser-induced ionization to detect soot inception in premixed flames

Samuel L. Manzello, Eui Ju Lee, and George W. Mulholland

Experimental measurements of laser-induced ionization were performed for ethene–air premixed flames operated near the soot inception point. Soot was ionized with a pulsed laser operated at 532 nm. The ionization signal was collected with a tungsten electrode located in the postflame region. Ionization signals were collected by use of both single-electrode and dual-electrode configurations. Earlier laser-induced-ionization studies focused on the use of a single biased electrode to generate the electric field, with the burner head serving as the path to ground. In many practical combustion systems, a path to ground is not readily available. To apply the laser-induced-ionization diagnostic to these geometries, a dual-electrode geometry must be employed. The influence of electrode configuration, flame equivalence ratio, and flame height on ionization signal detection was determined. The efficacy of the laser-induced-ionization diagnostic in detecting soot inception in the postflame region of a premixed flame by use of a dual-electrode configuration was investigated. Of the dual-electrode configurations tested, the dual-electrode geometry oriented parallel to the laser beam was observed to be most sensitive for detecting the soot inception point in a premixed flame. © 2005 Optical Society of America

OCIS codes: 120.0120, 120.1740.

1. Introduction

Soot is a common by-product that results from the combustion of fossil fuels. Release of soot into the atmosphere by combustion contributes to environmental and health hazards. Sooting represents incomplete combustion and can lead to hardware fouling. Soot formation is desirable in certain applications such as industrial furnaces, however, because the presence of soot greatly enhances radiative heat transfer. The challenge is to be able to control soot formation for a specific task. This requires a detailed understanding of the soot-formation process.

Unfortunately, understanding the mechanisms that are responsible for soot formation remains a daunting task. The major steps in soot formation consist of fuel pyrolysis, polycyclic aromatic hydrocarbon formation, particle inception, coagulation, surface growth, carbonization, agglomeration, and oxidation.[1–3] The process of soot inception is the least understood aspect of soot formation.

An effort is under way at the National Institute of Standards and Technology (NIST) to understand the complex soot-inception process. A well-stirred reactor (WSR) coupled with a plug-flow reactor has been built, and it will be used to study polycyclic aromatic hydrocarbon growth and soot inception.[4] For a given fuel–air system, there will be a unique fuel-to-air equivalence ratio corresponding to soot inception. The plan is to determine this critical point and to characterize the species concentration in the vicinity of this point with and without the addition of specific polycyclic aromatic hydrocarbons in the transition region between the well-mixed and plug-flow reactors. To this end, a laser-based diagnostic is desired for implementation within the WSR to quantitatively determine the soot-inception point during reactor operation.

Various laser-based diagnostics, such as laser-induced incandescence, laser-induced fluorescence, laser extinction, laser scattering, and laser-induced ionization, have been used to study soot formation in flames. Laser-induced ionization is an attractive diagnostic for soot-inception studies because it is a technique that has been used to detect small soot particles ($\approx$2 nm) and atomic ions in premixed flames.[5,6] The advantage of the laser-induced-ionization technique is that a sampling line is not

S. L. Manzello (samuel.manzello@nist.gov) and G. W. Mulholland are with the Building and Fire Research Laboratory, National Institute of Standards and Technology, Gaithersburg, Maryland 20899-8662. E. J. Lee is with the Fire and Engineering Service Research Department, Korea Institute of Construction and Technology, II-San City, South Korea.

Received 23 November 2004; revised manuscript received 11 March 2005; accepted 11 March 2005.

0003-6935/05/245105-07$15.00/0

© 2005 Optical Society of America

required for detecting soot inception in premixed flames. Recent work[7,8] has employed a dilution probe coupled with a nanodifferential mobility analyzer to measure incipient soot-particle size distributions in premixed flames. These studies have clearly shown that the magnitude of the dilution process can influence the particle size distributions.

For the laser-induced-ionization diagnostic, signals are produced on pulsed laser ionization in an electric field generated by a biased electrode. The electrons and ions move in opposite directions in the applied electric field, inducing a current that can be detected.[9] The electron signal is observed first, with the subsequent ion signal detected later in time. From mobility measurements of the ions produced, the molecular weight of the ions was estimated to be ≈2300 to ≈6000 amu. Spherical particles were assumed, resulting in a soot particle size of 1.6–2.2 nm. It is important to note that, for the laser-induced-ionization diagnostic, the ionization signals were observed precisely at the soot-inception point. At these equivalence ratios, only small particles exist.[10,11] Accordingly, based on the laser energies used and the corresponding beam diameters, such conditions were more than sufficient to raise a 1.6–2.2 nm particle well above the temperature required for thermal ionization. Thus the ionization signals reported were thought to arise from laser-induced heating of 2 nm particles followed by thermal ionization.[5]

In previously published studies a single biased electrode was used to generate the electric field, with the burner head serving as the path to ground.[5] In the WSR, as well as in many other practical combustion systems, a path to ground is not readily available. Accordingly, to apply the laser-induced-ionization diagnostic to these geometries, a dual-electrode geometry must be employed. In the dual-electrode geometry, one electrode is biased and other is grounded. Such geometry has been used to measure H and C atom concentrations in flames.[12]

The laser-induced-ionization technique has not received a great deal of attention in the literature. One reason for this may be that the technique has been applied only to limited geometries. This is unfortunate because this technique is a unique method for detecting incipient soot particles with diameters of ~2 nm. The method has not been applied to the study of soot inception, even though it has superior potential.

Therefore our goal in this study was to perform laser-induced-ionization measurements in the post-flame region of a premixed flame by using both the single- and dual-electrode configurations. The single-electrode geometry coupled with the premixed flame was selected for comparison to previously published laser-induced-ionization measurements. The premixed burner was used as a surrogate for other combustion systems, including the WSR. Finally, we employed a dual-electrode geometry to gauge the ability of the laser-induced-ionization diagnostic to determine the soot-inception point in a premixed flame.

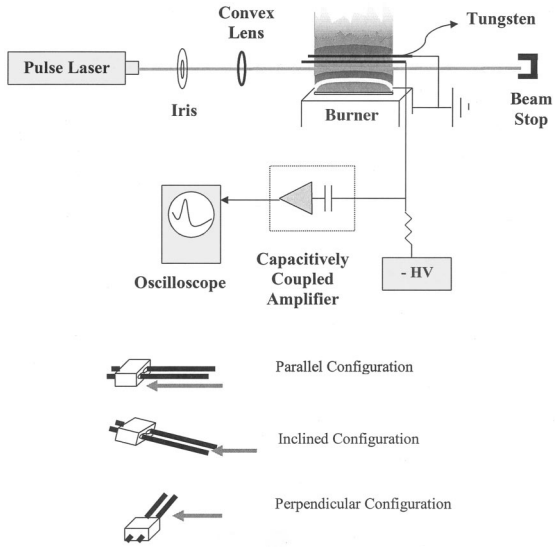

Fig. 1. Schematic of experimental apparatus displaying a burner, laser beam alignment, electronics for ionization signal detection, and dual-electrode configurations. HV, high voltage.

2. Experimental Description

Figure 1 displays the experimental apparatus. The pulsed laser source was a Continuum Nd:YAG system (≈5 ns pulse width) operating at a frequency-doubled wavelength of 532 nm. (We identify certain commercial equipment in this paper to accurately describe the experimental procedure, this in no way implies recommendation by the NIST.) The laser beam was aligned parallel to the burner slot and was focused to the center of the flame by a 200 mm convex lens. An iris was located in front of the focusing lens to block reflections, and the beam was terminated by use of a beam stop.

Premixed ethene–air flames were generated on a Perkin-Elmer slot burner with a slit length of 5 cm. This burner type has often been used for atomic absorption measurements. The Venturi orifice was set to allow no flow into the burner. Ethene was selected as the fuel because it is the fuel to be used for the NIST WSR experiments. The air flow rate was fixed and the fuel flow rate was varied near the soot-inception point for all experiments. All flow rates were controlled by mass-flow controllers with an uncertainty of 5%. The equivalence ratio reported corresponds to the fuel–air mixture into the burner. Under these conditions, the equivalence ratio at the sooting threshold was 2.5. This corresponds to a C/O ratio of 0.83. The burner was not equipped with a co-flow system of inert gas; thus one should consider the entrainment and diffusion of ambient air to know the exact composition of flame gases. The visible flame height was observed to be ≈10 cm above the burner head. The primary reaction zone, which was due to blue–green emission from C_2, was observed to be ≈4 mm above the burner head. For both single- and dual-electrode configurations, all measurements were performed downstream of the primary reaction zone.

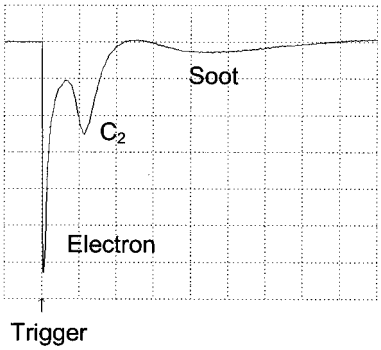

Fig. 2. Typical waveform traced by an oscilloscope: The time scale (x axis) is 20 μs/division and the amplitude scale (y axis) is 10 mV/division. The trigger signal of the pulsed laser is marked by a small arrow. Experimental conditions: $\phi = 2.7$; laser energy, 0.5 mJ/pulse; electrode biased at −300 V; single-electrode configuration. One hundred waveforms were averaged to reduce noise.

For the single-electrode configuration experiments, laser-induced-ionization signals were collected by use of a 1 mm diameter (6 cm length) tungsten electrode that was inserted into the flame above the laser beam. The electrode was mounted parallel to the laser beam and the flame, at a location within 1–2 mm above the laser beam. This geometry is known to produce the strongest ionization signals because the signal is collected over the entire length of the flame.[5,6] The electrode voltage was varied from −300 to −900 V.

The dual-electrode configuration consisted of two electrodes (each 0.56 mm in diameter and of 6 cm length) spaced 0.5 mm apart by a ceramic thermocouple insulator. For the dual-electrode–laser-beam geometry, the following positions were used: (1) parallel, laser beam below the electrodes, (2) perpendicular, laser beam below the electrodes, and (3) parallel, laser beam between the electrodes (inclined). One electrode was biased and other was grounded. The biased electrode voltage varied from −300 to −900 V.

In both the single- and dual-electrode configurations, the current through the electrode was converted to voltage by use of a capacitively coupled amplifier, which was identical to the device used in previous experiments.[5] Ionization signals were monitored with both digital and analog oscilloscopes, with time resolutions of 275–300 MHz. The ion signal's intensity and arrival time were measured with the digital oscilloscope; in which the trigger signal was synchronized to that of the laser. One hundred waveforms were averaged to reduce noise.

3. Results and Discussion

Figure 2 displays a characteristic waveform traced by the oscilloscope in the laser-induced-ionization experiments. The x axis indicates the time scale, 20 μs per division, and the y axis indicates the amplitude, 10 mV per division. This particular trace was generated with the single-electrode configuration, but the dual-electrode configuration produced a similar waveform. Three peaks were visible in the oscilloscope trace when the 532 nm laser source was used. The electron peak, which was quickest to arrive at the electrode, was produced soon after the trigger signal. The second peak, with an arrival time of 22 μs was smaller in magnitude than the electron signal. The third peak, with an arrival time of 90 μs, had the broadest range of ion arrival times.

The measured arrival times of the second and third peaks were observed to vary with electric field strength and laser-beam-to-electrode separation distance. These signals were observed only under fuel rich conditions and in those locations where soot was present. Therefore, one of these peaks was assigned as arising from ionized soot particles.

The three peaks in the oscilloscope trace were different from the two peaks previously published in laser-induced-ionization experiments.[5] To quantitatively assign the second and third peaks in the oscilloscope trace, we compared the arrival times of ions with those in previous experiments.[5] From kinetic theory, ion mobility K can be expressed as follows[13]:

$$K = \frac{3e}{16N}\sqrt{\frac{1}{m}+\frac{1}{M}}\sqrt{\frac{2\pi}{kT}}\frac{1}{\Omega_D}, \tag{1}$$

where m is the ion mass, M is the mass of the neutral carrier, N is the number concentration, T is temperature, and Ω_D is the average collision cross section. From Eq. (1), the ion mobility is a function of ion mass and the average collision cross section. The average collision cross section is dependent on an effective ion size parameter. Unfortunately, it is difficult to determine an effective ion size parameter for most ions. As a result, many investigators have assumed that the volume of the ion is proportional to its mass and have introduced mass-mobility correlations to assign various ions from mobility data.[14] This assumption is known to be valid for various hydrocarbon ions but breaks down for heavy polyatomic ions, as the mass dependence on ion mobility becomes weaker as m is much larger than M.

Compared with those in previous laser-induced-ionization experiments,[5] the laser wavelength and the laser energy per pulse were different. It has already been established in the literature that C_2 and C_3 fragments are produced on irradiation of soot particles.[15–17] It was observed that the second peak had an arrival time similar to that of sodium ions, Na^+. Details of the sodium ion arrival experiments are available elsehwhere.[5] Therefore, based on the mass-mobility correlations,[6] the second peak was assigned as arising from C_2^+ ions, as the mobility was expected to be close to that of sodium ions. The atomic weight of sodium is 23, versus 24 for C_2^+. With the Swan system of C_2 overlapping at 532 nm,[18] C_2 was easily ionized during the laser pulse.

Figure 3 displays the electron signal as a function of laser energy (energy/pulse) for both sooting and nonsooting ethene–air flames. We generated the data by using the single-electrode configuration for com-

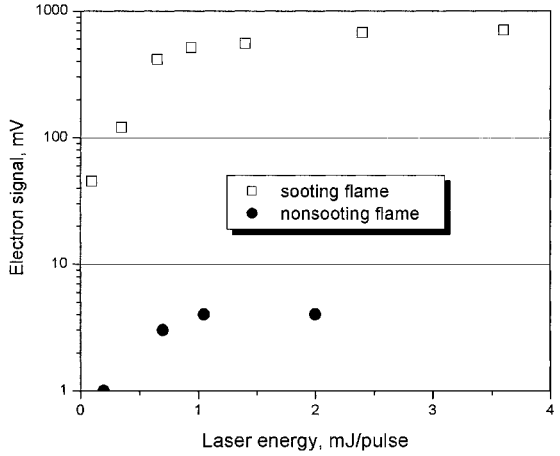

Fig. 3. Electron signal (the first peak) as a function of laser energy for both sooting (ϕ = 2.7) and nonsooting (ϕ = 2.3) flame stoichiometry. Single-electrode configuration.

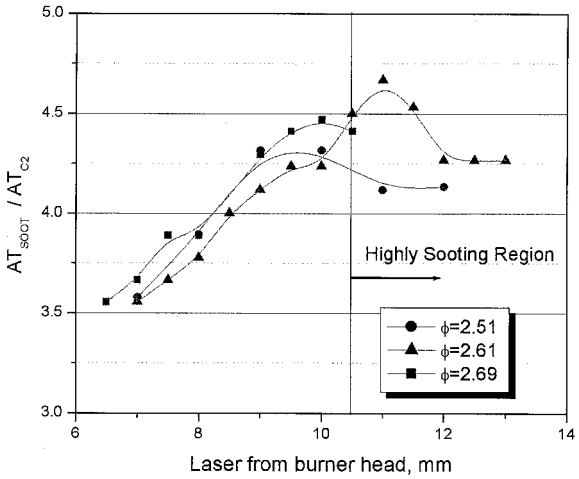

Fig. 4. Ratio of soot ion arrival time to C_2^+ ion arrival time as a function of flame height. Experimental conditions: laser energy, 0.7 mJ/pulse; single-electrode configuration; electrode biased at −700 V.

parison with previous work. Clearly, the electron signal was dependent on laser energy up to ≈1 mJ/pulse. For laser energy greater than 1 mJ/pulse, the electron signal was observed to saturate. A similar dependence on electron signal with laser energy was observed in previous experiments.[5] The influence of laser energy on the arrival time of ions was also investigated. As expected, the arrival times of C_2^+ and soot ions were observed to be independent of laser energy over the range of 0.15–3.6 mJ/pulse.

Under nonsooting conditions, the influence of the flame on the electron signal was minimal. The magnitude of the electron signal was, at maximum, 1% of the electron signal for the sooty flame. The influence of the flame on the measured electron signal was negligible and did not depend on laser energy (see Fig. 3).

The ion mobility can be characterized by use of low-field behavior, which implies that the mobility is independent of the electric field.[5,6] The average velocity of an ion in a gas is called the drift velocity, v_d, and is directly proportional to the electric field intensity, E, provided that $v_d = KE$. The proportionality coefficient, K, is defined as ion mobility. Measurements of ion arrival times can be used to deduce ion mobilities.[5,6]

Figure 4 displays the ratio of soot ion arrival time to C_2^+ ion arrival time as a function of laser-beam–burner-head distance for three equivalence ratios. The electrode–laser-beam distance was fixed. The data were obtained with the single-electrode configuration with the electrode biased at −700 V. As the laser-beam–burner-head distance was increased to 1 cm, the arrival times of soot ions were observed to increase while the arrival times of C_2^+ ions remained relatively constant. This trend suggests that as measurements are made higher in the flame, for a fixed equivalence ratio the mass of soot ions increases, resulting in increased soot ion arrival time. This would be expected, as soot particles are known to increase in size as one moves to greater heights (away from the soot-inception point) in a premixed flame. Eventually, as the measurements were made higher in the flame (1 cm from burner head), significant soot was observed to be deposited on the electrodes, producing difficulties in detection of ionization signals.

When the dual-electrode geometry was employed, the optical setup was identical to that of the single-electrode experiments. The following three electrode geometries were considered: (1) parallel, laser beam below the electrodes, (2) perpendicular, laser beam below the electrodes, (3) and parallel, laser beam between the electrodes (inclined). The inclined parallel electrode configuration was considered so that the laser beam could be placed close to the electrodes without striking the electrode holder. All three of these configurations are illustrated in Fig. 1. To determine the optimum configuration for detection of the ionization signals, the performance of these geometries was considered individually.

The influence of laser energy and biased electrode voltage on the electron signal intensity was investigated for the dual-electrode geometries and is displayed in Fig. 5. In the figure, the abbreviations SF and NSF denote sooting flame and nonsooting flame, respectively. It was observed that the lower the biased electrode voltage, the faster the electron signal was observed to saturate. The electron signal intensity had the following order: parallel > inclined > perpendicular. From the figure, the influence of the flame was deduced as a function of electrode geometry. The effect of biased electrode voltage on background noise was negligible compared with the influence of laser energy. The maximum signal-to-noise ratio was different for each electrode configuration, and we observed to be the following maximum ratios: perpendicular, 33; parallel, 17; inclined, 5. Thus the electrode configuration oriented perpendicular to the laser beam produced the best signal-to-noise ratio of the three geometries.

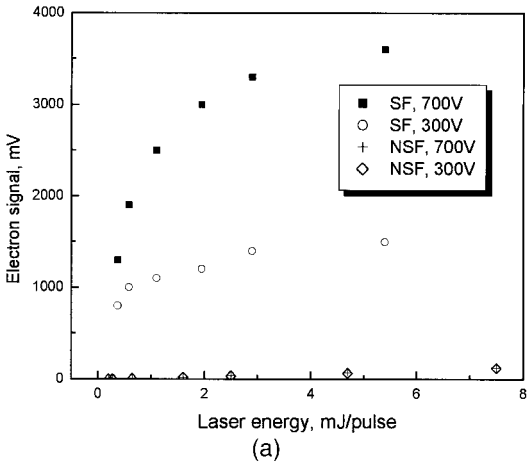

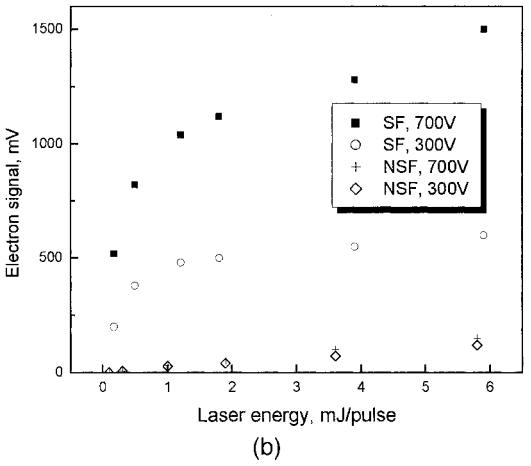

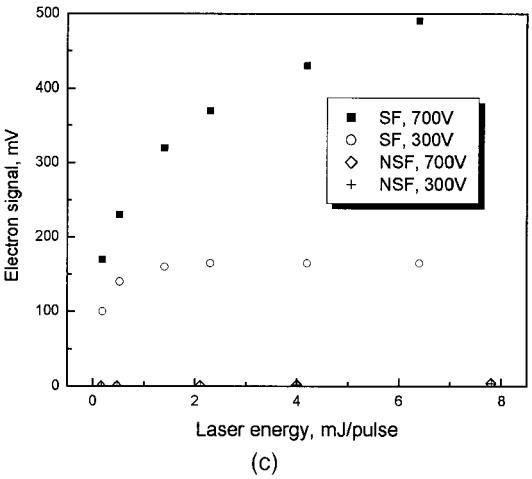

Fig. 5. Influence of laser energy and biased electrode voltage on electron signal intensity for three dual-electrode configurations: (a) parallel, (b) inclined, (c) perpendicular. SF, sooting flame; NSF, nonsooting flame.

It was observed that the arrival times of the soot and C_2^+ ionization signals varied depending on the dual-electrode configuration tested. The reason for this is that the ion arrival time depends on the local electric field and laser-beam-to-electrode distance. Altering the electrode configuration alters the electric field. The parallel electrode configuration provided the broadest range in time of the appearance of C_2^+ and soot ion signals of the three configurations.

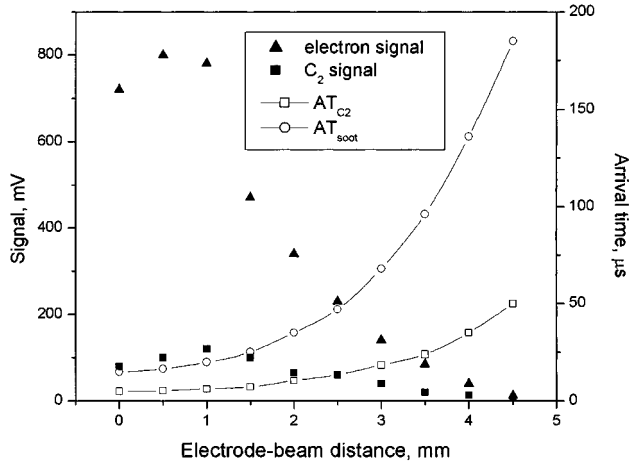

Fig. 6. Effect of electrode–laser-beam distance on the peak amplitude and arrival time of ions. Experimental conditions: $\phi = 2.69$; laser energy, 0.6 mJ/pulse; electrode biased at −500 V; laser beam 1 cm above burner head.

Figure 6 displays the electron and C_2^+ ionization signal magnitude and arrival time of soot and C_2^+ ions as a function of laser-beam-to-electrode distance for fixed stoichiometry into the burner. The data were obtained with a dual-electrode configuration oriented parallel to the laser beam. The electrode was biased at −500 V. As the electrode was moved further away from the laser beam, the strength of the electron and C_2^+ ionization signals decreased. In addition, the time for soot and C_2^+ ions to arrive at the electrode increased with a further separation of the laser-beam-to-electrode distance. In these experiments, a negative voltage was applied to the electrode. The soot and C_2^+ ions were generated at the location where the laser beam passed through the premixed flame. Therefore, if the laser-beam–burner-head distance was fixed and the distance from the laser beam to the electrode was increased, if the ions were positive it would be expected that the time for the ions to arrive at the electrode would increase with further laser-beam–electrode separation. These observations were confirmed in Fig. 6, and this suggests that these are indeed positive ions.

Based on the parametric investigation, the electron signal should be used in the dual-electrode geometry as an indication of soot inception. The electron signal was detected as rapidly as the electronics would allow and did not vary as a function of time for different electrode voltages and laser-beam-to-electrode distances. Furthermore, the electron signal displayed the largest magnitude of detected ionization signals. The electrode geometry oriented parallel to the laser beam provided the strongest electron signals. The perpendicular configuration provided electron signals as well, albeit weaker in magnitude than the parallel geometry. However, of the configurations investigated, the perpendicular electrode configuration

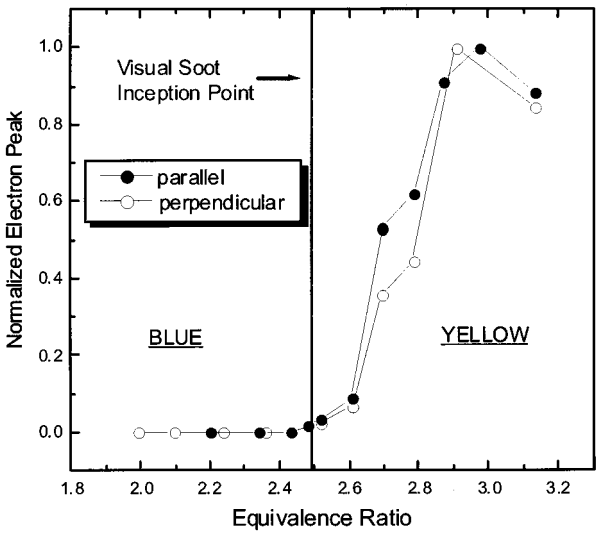

Fig. 7. Variation of normalized electron signal intensity as a function of equivalence ratio for parallel and perpendicular electrode configurations. Electrode biased at −700 V.

provided the best spatial resolution and signal-to-noise ratio. In addition, the perpendicular electrode configuration provided the simplest setup for use in practical combustion systems, such as the WSR. For the configuration with the laser beam placed between the electrodes, careful alignment was required for strong signals to be obtained. This requirement may result in difficulties when one is applying this configuration to combustion systems such as the WSR, because small alignment modifications would result in large signal fluctuations.

To gauge the ability of the laser-induced ionization diagnostic to detect the onset of sooting in a premixed flame, we plotted the normalized electron signal as a function of equivalence ratio, as shown in Fig. 7. The following experimental procedure was adopted for the perpendicular electrode configuration: The electrode–laser-beam distance was fixed (2 mm) and the burner head was varied until a signal was detected at the visual soot-inception point. The visual soot-inception point was defined as the first visible observation of yellow luminosity just above the reaction zone. The reaction zone was characterized by blue–green emission from C_2. The fuel flow rate was then increased, and the electron signal was recorded as a function of equivalence ratio. A similar procedure was performed for the parallel electrode configuration. The biased electrode voltage was fixed at −700 V for each electrode configuration.

The parallel electrode configuration was the most sensitive in determining the soot-inception point. For certain applications, the parallel electrode configuration may not be possible. The perpendicular electrode configuration may still provide quantitative information on the soot-inception point in a premixed flame. These results demonstrate that the laser-induced-ionization diagnostic can be used to detect the onset of soot inception in a premixed flame.

4. Conclusions

Experimental measurements of laser-induced ionization were performed for ethene–air premixed flames operated near the soot-inception point. Ionization signals were collected with both single-electrode and dual-electrode configurations. Earlier laser-induced-ionization studies focused on the use of a single biased electrode to generate the electric field, with the burner head serving as the path to ground. In many practical combustion systems, a path to ground is not readily available. To apply the laser-induced-ionization diagnostic to these geometries, one must employ a dual-electrode geometry. The influence of electrode configuration, flame equivalence ratio, and flame height on ionization signal detection was determined.

The following three dual-electrode geometries were considered: (1) parallel, laser beam below the electrodes, (2) perpendicular, laser beam below the electrodes, and (3) parallel, laser beam between the electrodes (inclined). Based on the parametric investigation, the electron signal should be used as an indication for soot inception by use of the dual-electrode geometry. The electron signal displayed the largest magnitude of detected ionization signals. The parallel electrode geometry provided the strongest electron ionization signals. The perpendicular configuration provided electron ionization signals as well, albeit weaker in magnitude than the parallel geometry. However, of the configurations investigated, the perpendicular configuration electrode configuration does provide the best spatial resolution and signal-to-noise ratio. The perpendicular electrode configuration provided the simplest setup for use in practical combustion systems. For the configuration with the laser beam placed between the electrodes, careful alignment was required for strong signals. This requirement may result in difficulties when one is applying this configuration to combustion systems because small alignment modifications would result in large signal fluctuations. The dual-electrode geometry oriented parallel to the laser beam was observed to be most sensitive to detect the soot-inception point in a premixed flame.

This study was supported by the U.S. Department of Defense through the Strategic Environmental Research and Development Program; Charles Pellerin is the program manager. We acknowledge helpful suggestions and guidance from Kermit C. Smyth during the course of this work; in addition, he reviewed the manuscript and provided suggestions to strengthen the paper. The assistance of Marco G. Fernandez with the experimental setup was crucial in performing the experiments and is greatly appreciated.

References

1. I. Glassman, “Soot formation in combustion process,” Proc. Combust. Inst. **22,** 295–311 (1988).
2. H. Richter and J. B. Howard, “Formation of polycyclic aromatic hydrocarbons and their growth to soot—a review of chemical reaction pathways,” Proc. Combust. Inst. **26,** 565–608 (2000).
3. I. M. Kennedy, “Models of soot formation and oxidization,” Prog. Energy Combust. Sci. **23,** 95–132 (1997).

4. S. L. Manzello, G. W. Mulholland, M. Donovan, W. Tsang, K. Park, and M. Zachariah, "On the use of a well stirred reactor to study soot inception," presented at the Fourth Joint Meeting of the U.S. Sections of the Combustion Institute, Philadelphia, Pa., 20–23 March, 2005.
5. K. C. Smyth and W. G. Mallard, "Laser-induced ionization and mobility measurements of very small particles in premixed flames at the sooting limit," Combust. Sci. Technol. **26,** 35–41 (1981).
6. W. G. Mallard and K. C. Smyth, "Mobility measurements of atomic Ions in flames using laser-enhanced ionization," Combust. Flame **44,** 61–70 (1982).
7. B. Zhao, Z. Yang, J. Wang, M. Johnston, and H. Wang, "Analysis of soot particles in a laminar premixed ethylene flame by scanning mobility particle sizer," Aerosol Sci. Technol. **37,** 611–620 (2003).
8. M. M. Maricq, "Size and charge of soot particles in rich premixed ethylene flames," Combust. Flame **137,** 340–350 (2004).
9. J. C. Travis and G. C. Turk, *Laser-Enhanced Ionization Spectrometry* (Wiley, 1996).
10. A. D'Alessio, A. Di Lorenzo, A. Borghese, F. Beretta, and S. Masi, "Study of soot nucleation zone of rich methane–oxygen flames," Proc. Combust. Inst. **16,** 695–703 (1977).
11. B. S. Haynes, and H. Gg. Wagner, "Optical studies of soot-formation processes in premixed flames," Ber. Bunsenges. Phys. Chem. **84,** 585–610 (1980).
12. K. C. Smyth and P. J. H. Tjossem, "Relative H-atom and C-atom concentration measurements in a laminar, methane/air diffusion flame," Proc. Combust. Inst. **23,** 1829–1837 (1990).
13. G. W. Griffin, I. Dzidic, D. I. Carroll, R. N. Stilwell, and E. C. Horning, "Ion mass assignments based on mobility measurements," Anal. Chem. **45,** 1204–1209 (1973).
14. S. N. Lin, G. W. Griffin, E. C. Horning, and W. E. Wentworth, "Dependence of polyatomic ion mobilities on size," J. Chem. Phys. **60,** 4994–4999 (1974).
15. C. R. Shaddix and K. C. Smyth, "Laser-induced incandescence measurements of soot production in steady and flickering methane, propane, and ethylene diffusion flames," Combust. Flame **107,** 418–452 (1996).
16. P. Bengtsson and M. Aldén, "Optical investigation of laser-produced C_2 in premixed soot ethylene flames," Combust. Flame **80,** 322–328 (1990).
17. A. C. Eckbreth and R. J. Hall, "CARS thermometry in a sooting flame," Combust. Flame **36,** 87–98 (1979).
18. R. W. B. Pearse and A. G. Gaydon, *The Identification of Molecular Spectra*, 4th ed. (Chapman & Hall, 1976).